Journal Pre-proof

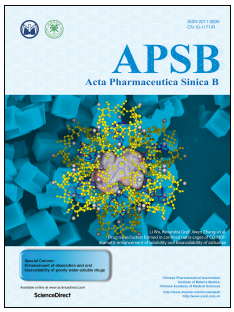

Discovery of a novel AhR–CYP1A1 axis activator for mitigating inflammatory diseases using an *in situ* functional imaging assay

Feng Zhang, Bei Zhao, Yufan Fan, Lanhui Qin, Jinhui Shi, Lin Chen, Leizhi Xu, Xudong Jin, Mengru Sun, Hongping Deng, Hairong Zeng, Zhangping Xiao, Xin Yang, Guangbo Ge

PII: S2211-3835(24)00379-4

DOI: https://doi.org/10.1016/j.apsb.2024.09.014

Reference: APSB 2135

To appear in: *Acta Pharmaceutica Sinica B*

Received Date: 15 August 2024

Revised Date: 12 September 2024

Accepted Date: 13 September 2024

Please cite this article as: Zhang F, Zhao B, Fan Y, Qin L, Shi J, Chen L, Xu L, Jin X, Sun M, Deng H, Zeng H, Xiao Z, Yang X, Ge G, Discovery of a novel AhR–CYP1A1 axis activator for mitigating inflammatory diseases using an *in situ* functional imaging assay, *Acta Pharmaceutica Sinica B*, https://doi.org/10.1016/j.apsb.2024.09.014.

ORIGINAL ARTICLE

Discovery of a novel AhR–CYP1A1 axis activator for mitigating inflammatory diseases using an *in situ* functional imaging assay

Feng Zhang[a,†], Bei Zhao[a,†], Yufan Fan[a], Lanhui Qin[a], Jinhui Shi[a], Lin Chen[a], Leizhi Xu[a], Xudong Jin[b], Mengru Sun[a], Hongping Deng[a], Hairong Zeng[a], Zhangping Xiao[c], Xin Yang[d], Guangbo Ge[a,*]

[a]*Shanghai Frontiers Science Center of TCM Chemical Biology, Institute of Interdisciplinary Integrative Medicine Research, Shanghai University of Traditional Chinese Medicine, Shanghai 201203, China*

[b]*St Hilda's College, Oxford University, Oxford OX4 1DY, UK*

[c]*Department of Chemistry, Imperial College London, London W12 0BZ, UK*

[d]*Department of Electrical and Electronic Engineering, School of Engineering, Cardiff University, Cardiff CF24 3AA, UK*

Received 15 August 2024; received in revised form 12 September 2024; accepted 13 September 2024

[*]Corresponding author.

E-mail address: geguangbo@shutcm.edu.cn (Guangbo Ge).

[†]These authors made equal contributions to this work.

Running title: Discovering AhR-CYP1A1 axis activators using an *in situ* functional imaging assay

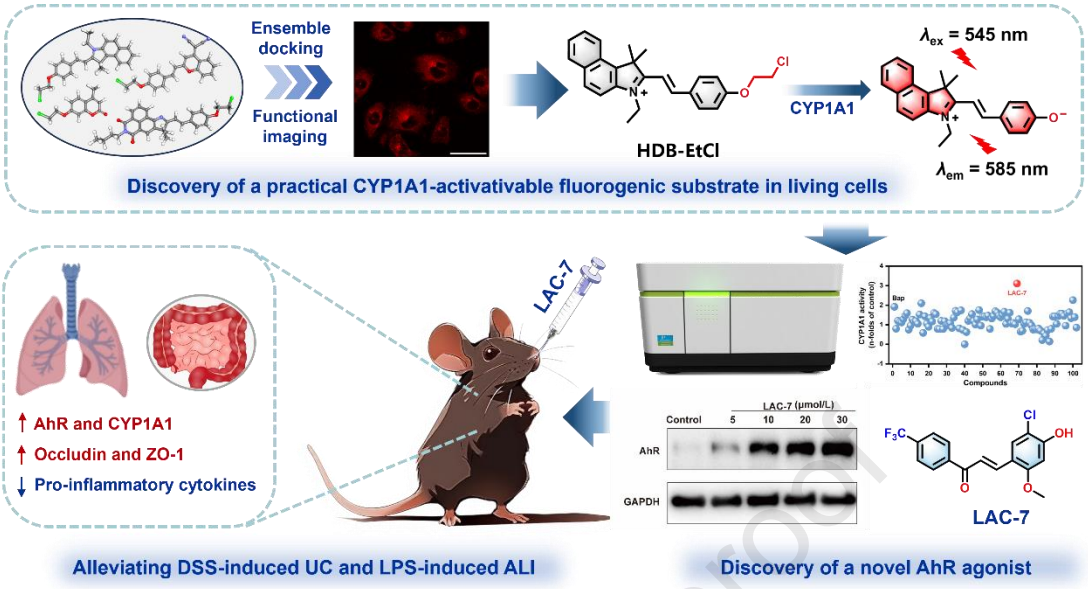

An optimized fluorometric cell-based assay was devised for *in situ* functional imaging of CYP1A1 activities in living systems, which was used for discovering efficacious AhR-CYP1A1 axis activators as novel anti-inflammatory agents.

Abstract The aryl hydrocarbon receptor (AhR) plays a crucial role in regulating many physiological processes. Activating the AhR–CYP1A1 axis has emerged as a novel therapeutic strategy against various inflammatory diseases. Here, a practical *in situ* cell-based fluorometric assay was constructed to screen AhR-CYP1A1 axis modulators, *via* functional sensing of CYP1A1 activities in live cells. Firstly, a cell-permeable, isoform-specific enzyme-activable fluorogenic substrate for CYP1A1 was rationally constructed for *in-situ* visualizing the dynamic changes of CYP1A1 function in living systems, which was subsequently used for discovering the efficacious modulators of the AhR–CYP1A1 axis. Following screening of a compound library, **LAC-7** was identified as an efficacious activator of the AhR–CYP1A1 axis, which dose-dependently up-regulated the expression levels of both CYP1A1 and AhR in multiple cell lines. **LAC-7** also suppressed macrophage M1 polarization and reduced the levels of inflammatory factors in LPS-induced bone marrow-derived macrophages. Animal tests showed that **LAC-7** could significantly mitigate DSS-induced ulcerative colitis and LPS-induced acute lung injury in mice, and markedly reduced the levels of multiple inflammatory factors. Collectively, an optimized fluorometric cell-based assay was devised for *in situ* functional imaging of CYP1A1 activities in living systems, which strongly facilitated the discovery of efficacious modulators of the AhR–CYP1A1 axis as novel anti-inflammatory agents.

KEY WORDS Aryl hydrocarbon receptor (AhR); Cytochrome P450 1A1 (CYP1A1); *In situ* functional imaging; Ulcerative colitis (UC); Acute lung injury (ALI); Long term imaging; Rational design; Inflammatory diseases

1. Introduction

The aryl hydrocarbon receptor (AhR), a vital member of the Per-ARNT-Sim-basic helix–loop–helix protein family of transcription factors, is widely expressed in immune, epithelial, endothelial, and stromal cells within mammalian barrier organs[1-3]. Emerging evidence has suggested that AhR plays crucial roles in regulating various physiological processes, such as xenobiotic metabolism[4], cell development and differentiation[4,5], as well as stem cell maintenance[4]. Additionally, AhR is implicated in multiple diseases, including inflammation[1,6], metabolic disorders[7], cancer[1,3,7], and autoimmune diseases[1,7]. As a canonical ligand-activated transcription factor, AhR can be activated by a wide range of structurally diverse chemicals, including endogenous metabolites (such as arachidonic acid metabolites), phytochemicals (such as flavonoids), therapeutic drugs, and environmental pollutants[8-11]. Upon ligand binding, AhR undergoes a conformational change that exposes its N-terminal nuclear localization sequence, facilitating the translocation of the AhR chaperone complex to the nucleus. Once inside the nucleus, AhR dimerizes with the aryl hydrocarbon receptor nuclear translocator protein (ARNT). This complex then binds to the AhR-responsive enhancer elements (AHREs) in the 5′ regulatory regions of AhR-driven genes, activating the transcription of various target genes, including the genes encoding xenobiotic-metabolizing enzymes (such as *CYP1A1* and *CYP1B1*)[2,12,13].

As one of the most well-characterized gene products of the AhR signaling pathway, CYP1A1 has drawn significant attention in the fields of inflammation, immunity, cancer, and other metabolic diseases[14-16]. Upon activation of AhR signaling, both the transcription and expression levels of CYP1A1 can be up-regulated. The upregulated CYP1A1 can further catalyze the oxidative metabolism of a variety of endogenous substances (such as estradiol) and therapeutic agents, including AhR modulators, constituting complex regulatory networks between AhR and its gene products, as well as their regulators[17-22]. Moreover, it has been reported that activating the AhR signaling cascade can trigger the up-regulation of AhR repressor (AhRR), a protein capable of competing with AhR for ARNT, thus resulting in a negative feedback regulation that suppresses sustained transcriptional activation of AhR[23,24]. These findings demonstrate that regulating the AhR signaling cascade in living systems is extremely complex, making the practical *in situ* assays for high-throughput screening and

characterization of AhR modulators highly desirable.

Growing evidence has suggested that modulating the AhR–CYP1A axis is a double-edged sword[25]. On the one hand, several environmental toxins (such as aflatoxins, benzo[a]pyrene) can trigger carcinogenesis by activating the AhR–CYP1A axis[26-28], while direct blocking of AhR activation is a feasible strategy for preventing tumor progression in lung cancer[29]. On the other hand, the AhR–CYP1A axis has been validated as a therapeutic target for treating autoimmune inflammatory diseases. Activating this axis in specific cellular environments is emerging as a novel therapeutic strategy against various inflammatory diseases, including intestinal inflammation, skin inflammation, acute lung injury, and acute renal injury[6,30-33]. AhR–CYP1A axis agonists can migrate skin, intestine, and lung injuries by repairing the structure of epithelial tight junctions and up-regulating the expression of tight junction proteins through activating the AhR–CYP1A axis[31]. Therefore, it is urgent and necessary to develop reliable and practical assays for identifying and evaluating the efficacious modulators of the AhR–CYP1A1 axis in living systems.

Over the past few decades, the cell-based AhR luciferase reporter assay has been frequently used for the rapid screening of AhR activators[34,35]. This assay can efficiently assess the transcriptional activity of AhR upon binding with a tested ligand but cannot reflect the complex negative feedback mechanism of the up-regulated CYP1As by the tested ligand. In some cases, the transcriptional activity levels determined by the AhR luciferase reporter assay were inconsistent with the function levels of the downstream gene products of AhR, such as CYP1A1. This discrepancy suggests that the AhR luciferase reporter assay may not precisely characterize the interaction networks among AhR, CYP1As, and the small-molecule ligand. Given that CYP1A1 is a key downstream gene product and an important phenotypic marker of AhR activation, as well as a crucial mediator of various inflammatory diseases[36,37], *in situ* visualization of the dynamic changes of CYP1A1 function in living systems offers an alternative way for precisely assessing the end-point outcomes of the tested chemicals. Although a variety of fluorogenic substrates for CYP1A1 (Supporting Information Table S1) have been reported over the past decade, most of these probes suffer from poor isoform-specificity, limited sensitivity, poor solubility, and very poor cell-membrane permeability[38-40]. Moreover, most of the phenolic metabolites of CYP1A1 substrates can be

readily metabolized by phase II metabolizing enzymes (such as uridine 5'-diphospho-glucuronosyltransferases and sulfotransferases), or are easily transported to the extracellular matrix by the efflux pumps (such as p-glycoprotein, P-gp). Consequently, these substrates fail to generate stable fluorescent signals inside living cells for long-term *in situ* visualization[41-43]. These limitations strongly restrict their applications in real-time monitoring and *in situ* visualization of CYP1A1 activities in complex living systems.

To address the above shortcomings, a rational molecule design strategy combined with a cell-based screening approach was employed to identify a cell-permeable and isoform-specific fluorogenic substrate for *in-situ* functional imaging of CYP1A1 (Scheme 1). After ensemble docking screening and cell-based functional imaging screening, **HDB-EtCl** was selected as an optimized CYP1A1-activatable fluorogenic substrate, demonstrating an exceptional combination of isoform-specificity, rapid response, excellent cell-membrane permeability, and superior optical properties. **HDB-EtCl** was then used to develop a cell-based fluorometric assay for *in situ* functional imaging of CYP1A1 activity and for high-throughput screening of CYP1A1 modulators in living systems. Screening an in-house compound library led to the identification of **LAC-7** as a novel and effective CYP1A1 inducer, which was further validated as a potent activator of the AhR–CYP1A1 axis in various cells. The anti-inflammatory potentials of **LAC-7** were then evaluated in macrophages, dextran sulfate sodium (DSS)-induced ulcerative colitis (UC) mice, and lipopolysaccharide (LPS)-induced acute lung injury (ALI) mice.

2. Materials and methods

2.1. Chemicals and biological samples

All chemical reagents were supplied by Sinopharm Chemicals (Shanghai, China). Resorufin was purchased from J&K Scientific (Beijing, China). D-Glucose-6-phosphate (G-6-P), glucose-6-phosphate dehydrogenase (G-6-PDH), and β-$NADP^+$ were supplied by Sigma–Aldrich (St. Louis, MO, USA). $MgCl_2$ was provided by Sinopharm Chemical Reagent (Shanghai, China). Resveratrol was purchased from TCI (Shanghai) Development Co., Ltd.

Pooled human liver microsomes from 50 donors (HLMs, lot No. X008067) were obtained from Bioreclamation IVT (Baltimore, MD, USA). Ketoconazole, DMEM medium, RPMI 1640 medium, MEM medium, and PBS were sourced from Meilun Bio. Tech (Dalian, China). Fetal bovine serum (FBS) and trypsin were provided from Gibco (Thermo Fisher, Waltham, MA, USA). Hoechst 33342 was supplied by Shanghai Yuanye Biotechnology Co., Ltd. (Shanghai, China). The antibodies of AhR, ZO-1, and Occludin were supplied by Proteintech (Wuhan, China). Antibodies against CYP1A1, CD31, and GAPDH were purchased by Cell Signaling Technology (Beverly, MA, USA).

2.2. Cell-membrane permeability assay

The cell-membrane permeabilities of the fluorescent substrate candidates were assayed. In brief, BEAS-2B cells were cultured with the DMEM medium supplemented with 10% FBS in a humidified atmosphere of 5% CO_2 at 37 °C. When the cells reached about 80% confluency, the cells were trypsinized and then resuspended with the DMEM basal medium to the density of 2×10^5 cells/mL. Subsequently, 200 μL of the cell suspension was incubated with CYP1A1 candidate substrates (5 μmol/L) for 30 min at 37 ℃. Then, the cells were centrifuged (1000 rpm, 3 min, Fresco 21, Thermo Fisher, Waltham, MA, USA) and resuspended in DMEM basal medium, followed by another centrifugation to remove any residual CYP1A1 substrate candidates. After that, the cells were lysed with ice-cold methanol (200 μL) and centrifuged (20,000×*g*, 20 min, Fresco 21, Thermo Fisher, Waltham, MA, USA) at 4 °C. The supernatant was subsequently analyzed using HPLC-UV (LC-20A, Shimadzu, Kyoto, Japan).

2.3. Functional imaging of CYP1A1 in living cells

Several cells expressing high levels of CYP1A1 (BEAS-2B, H292, Caco2, HepG2 cells) were used for fluorescent imaging of **HDB-EtCl** using confocal laser scanning microscopy (Leica SP8, Wetzlar, Germany). H292 cells were cultured within the RPMI 1640 medium containing 10% FBS. Caco2 cells in MEM medium containing 20% FBS, and BEAS-2B and HepG2 cells in DMEM medium containing 10% FBS. All cells were cultured in a humidified atmosphere of 5% CO_2 at 37 °C. The cells were seeded in confocal dishes at a density of 1×10^5 cells per dish. After 24 h, when the cells completely adhered to the wall, the inhibitor

group was pre-incubated with resveratrol (100 μmol/L) for 1 h. Then, Hoechst 33342, **HDB-EtCl** (5 μmol/L) were added. Following incubation for 30 min, cells were washed 2–3 times with PBS, and the cell morphology was fixed with 4% paraformaldehyde. The fluorescent images were acquired using one-photon mode. The blue channel was at λ_{ex} 405 nm, λ_{em} 415–485 nm, and the red channel was at λ_{ex} 552 nm, λ_{em} 580–640 nm.

2.4. Functional imaging of CYP1A1 in mouse liver and lung slices

Mouse lung and liver slices were obtained from C57BL/6J mice. All experimental procedures were executed according to the protocols approved by the Animal Care and Use Committee of Shanghai University of Traditional Chinese Medicine (SHUTCM) with the approval number PZSHUTCM2303060002. After fixing the liver and lung tissue of the mouse, they were sliced into 150 μm sections with a freezing microtome and placed in confocal dishes with 2 mL PBS. The inhibitor group was pre-incubated with resveratrol (100 μmol/L) for 1 h, and Hoechst 33342, **HDB-EtCl** (5 μmol/L) were added. Following a 30 min incubation, fluorescent images were acquired using one-photon mode. The blue channel was at λ_{ex} 405 nm, λ_{em} 415–485 nm, and the red channel was at λ_{ex} 552 nm, λ_{em} 580–640 nm.

2.5. CYP1A1 induction assay

To screen the induction effects of Benzo[*a*]pyrene (Bap, a positive inducer of CYP1A1) and an in-house compound library on CYP1A1 in living cells, BEAS-2B cells were seeded in the black 96-well cell culture plates with clear bottom at a density of 1×10^4 cells per well. When the cells reached about 60% confluency, Bap (reported CYP1A1 inducers) and the in-house compound library (10 μmol/L) were added and cultured for 24 h. Subsequently, 100 μL **HDB-EtCl** (5 μmol/L) and Hoechst 33342 were added to initiate the reaction. Following incubation for 30 min, fluorescent images were performed using a high-content cell imaging analysis system (Operetta CLS, PE, Waltham, MA, USA). The blue channel was at λ_{ex} 355–385 nm, λ_{em} 430–500 nm, and the red channel was at λ_{ex} 530–560 nm, λ_{em} 570–650 nm.

*2.6. Anti-inflammatory effect of **LAC-7** in BMDMs*

Bone marrow was harvested from tibias and femurs using an aseptic technique, and the bone

marrow cells were flushed. The cells were cultured in Dulbecco's modified Eagle's medium fortified with 10% FBS and subjected to differentiation into bone marrow-derived macrophages (BMDM) cells using 40 ng/mL mouse Macrophage Colony-Stimulating Factor (M-CSF) for 6 days. To explore the effect of **LAC-7** on macrophage polarization, **LAC-7** (10 and 20 μmol/L) was introduced into the M1-stimulated medium (1 μg/mL LPS). BMDM cells were harvested and stained with CD86, CD206, and CD11b for 20 min, followed by triple washing. Subsequently, the anti-inflammation potentials were assessed using a flow cytometer (CytoFLEX S, Beckman, Brea, CA, USA). All experimental procedures were executed according to the protocols approved by the Animal Care and Use Committee of SHUTCM (approval number: PZSHUTCM2303060002).

*2.7. Safety and tolerability test of **LAC-7***

C57BL/6J mice (n = 12, 6 male and 6 female, weighing around 20 g) were housed under controlled environmental conditions (22 ± 2 °C; 55 ± 5% relative humidity; 12 h light/dark cycle) for one week with free access to food and water. **LAC-7** was suspended in water before oral administration. The mice were randomly divided into two groups (n = 6, water and **LAC-7**). Mice were orally administered **LAC-7**/water (100 mg/kg) continuously for 14 days, and their status was observed, and their weight was measured daily. After the last oral administration of **LAC-7**/water for 24 h, blood samples were collected to test the biochemical index, while the mice organs, including heart, liver, spleen, lung, kidney, large intestine, small intestine, and brain, were harvested for hematoxylin and eosin (H&E) staining to identify histopathological abnormalities.

*2.8. **LAC-7** relieved DSS-induced UC and LPS-induced ALI in mice*

2.8.1. Animals

Male C57BL/6J mice were obtained from the Experiment Animal Center (SHUTCM). All experimental procedures were executed according to the protocols approved by the Animal Care and Use Committee of SHUTCM (the approval number: PZSHUTCM2303060002). The animals were housed under a 12 h/12 h light/dark cycle, 22 ± 2 ℃ and 55 ± 5% relative

humidity for one week with free access to food and water.

2.8.2. Construction and treatment of ulcerative colitis (UC)

Mice were randomly divided into five groups of six mice per experimental condition. UC model mice were induced by adding 3% (*w*/*v*) DSS (MP Biomedical, Santa Ana, CA, USA) to the drinking water for 8 days, followed by normal drinking water for 2 days. The control group mice were housed with free access to food and water[44,45]. **LAC-7** (20 and 40 mg/kg) and salazosulfapyridine (SASP, a positive drug for ulcerative colitis, 200 mg/kg) were orally administered daily for 8 days, followed by normal drinking water for 2 days.

2.8.3. Construction and treatment of acute lung injury (ALI)

Mice were randomly divided into five groups: control, LPS (Sigma–Aldrich, St. Louis, MO, USA), **LAC-7** (20 mg/kg), **LAC-7** (40 mg/kg), and dexamethasone (Dex, a positive control for ALI). Three days prior to LPS induction, the **LAC-7** group mice received intragastric injections of 20 and 40 mg/kg per day, respectively, and the Dex group mice were orally administered Dex (5 mg/kg). Mice were anesthetized *via* intraperitoneal injection of avertin at a dose of 360 mg/kg. After anesthesia, the LPS group, **LAC-7** group, and Dex group mice were challenged with LPS (5 mg/kg) by intratracheal instillation[46,47]. After that, mice were moved to a heating pad to recover from anesthesia. After 9 h, all mice were euthanized.

2.8.4. Collection and analysis of bronchoalveolar lavage fluid (BALF)

To procure BALF, a sterile syringe containing 1 mL of saline was inserted into the trachea of the mice, and the lungs were flushed three times. Subsequently, the BALF in the syringe was collected and centrifuged (2500 rpm, 4 °C, 10 min, Fresco 21, Thermo Fisher, Waltham, MA, USA), and the supernatant was taken for subsequent analysis. The total protein contents in BALF were determined using a commercial bicinchoninic acid (BCA) Protein Assay Kit, and the cell counts in BALF were performed.

2.9. Data analysis

The data were estimated using GraphPad Prism V8.0 (GraphPad Software Inc., La Jolla, CA,

USA), ImageJ software (National Institutes of Health, Bethesda, MD, USA), and Origin 2021 (OriginLab Corporation, Northampton, MA, USA).

3. Results and discussion

3.1. Design and synthesis of CYP1A1-activable fluorogenic substrate candidates

The ideal enzyme-activatable fluorogenic substrates for *in situ* functional imaging of target enzyme(s) in living cells should meet the following requirements: 1) ultra-high specificity; 2) good cell-membrane permeability; and 3) a high turnover rate with substantial fluorescence emission enhancement. Furthermore, the corresponding fluorogenic metabolite should also meet the following requirements: 1) good photo- and chemo-stability; 2) a non-substrate for efflux transporters (*e.g.*, P-gp); and 3) excellent optical properties and favorable metabolic stability, enabling the metabolite to generate stable and bright fluorescence signals inside within live cells.

In previous studies, our group and colleagues have demonstrated that introducing a chloroethyl or isopropyl group to the phenolic group of certain fluorophores greatly improves the isoform-specificity of CYP1A1 substrates[38,39,48]. In this work, we designed a total of 24 CYP1A1-activatable fluorogenic substrate candidates by masking the phenolic group of the commonly used fluorophores (emission wavelength > 550 nm) with either a chloroethyl or isopropyl group (Supporting Information Fig. S1). Each candidate was then docked with six different crystal structures of human CYP1A1 (PDB Bank, 4I8V, 6DWM, 6DWN, 6O5Y, 6UDL, 6UDM) using ensemble docking (ED). As depicted in Fig. 1A and B, ten substrate candidates (No. 1–6, 11, 12, 17, and 18) showed high binding affinities with all investigated CYP1A1 crystal structures, implying their potential as fluorogenic substrates for CYP1A1.

Subsequently, ten fluorogenic substrate candidates (**RSF-ipr**, **RSF-EtCl**, **HDI-ipr**, **HDI-EtCl**, **HDB-ipr**, **HDB-EtCl**, **DCM-ipr**, **DCM-EtCl**, **TCF-ipr**, **TCF-EtCl**) and their dealkylated metabolites were synthesized and fully characterized using NMR and HRMS (Supporting Information Schemes S1–S5, Supporting Information Figs. S2–S29). Biotransformation assay showed that both **DCM-ipr** and **DCM-EtCl** could be converted into

multiple metabolites by hCYP1A1, while the other tested substrates were metabolized by hCYP1A1 into a single fluorescent product (the corresponding fluorophore). The metabolic rates (Supporting Information Table S2) of **RSF-ipr, RSF-EtCl, HDI-ipr, HDI-EtCl, HDB-ipr, HDB-EtCl, TCF-ipr, TCF-EtCl** in CYP1A1 were then determined by HPLC–UV, the results showed that the conversion rates of these substrates in CYP1A1 (following 30 min incubation) were exceeded 10%. These findings clearly demonstrate that all designed substrate candidates are indeed substrates for hCYP1A1, which encourages investigation of their *in-situ* imaging performance for sensing CYP1A1 in live cells.

*3.2. **HDB-EtCl** shows good in-situ imaging performance for CYP1A1 in live cells*

Next, the *in-situ* imaging performance of ten fluorogenic substrate candidates for functional imaging of CYP1A1 in live cells was carefully investigated. To achieve this, both CYP1A1 transiently transfected HEK293T cells and BEAS-2B cells (human normal lung epithelial cells that overexpressed CYP1A1) were stained with each tested fluorogenic substrate under identical conditions (5 μmol/L for 30 min incubation), while the enhancement in fluorescence emission was recorded using laser scanning confocal microscopy. As depicted in Fig. 1C and Supporting Information Figs. S30–S32, after co-incubation with **HDB-EtCl** or **HDB-ipr** for 30 min, bright red fluorescent signals were observed within the HEK293T cells overexpressed CYP1A1 and BEAS-2B cells. In contrast, very weak or uneven fluorescent signals were observed after co-incubation with other fluorogenic agents under identical conditions. These findings suggest that **HDB-EtCl** and **HDB-ipr** hold good *in-situ* imaging performance for CYP1A1.

Further investigations revealed that the cell membrane permeability of **HDB-EtCl** was slightly higher than that of **HDB-ipr** (20.52% *vs.* 18.17%), while the turnover rate of **HDB-EtCl** in CYP1A1 was significantly higher than that of **HDB-ipr** (Supporting Information Fig. S33 and Table S3). These findings will explain why **HDB-EtCl** exhibits good *in situ* imaging performance in BEAS-2B cells. Additionally, it was also found that **HDBI** showed good metabolic stability in phase II metabolic systems (Supporting Information Fig. S34), suggesting that **HDB-EtCl** offered a wide time window for *in situ* imaging of hCYP1A1 in live cells. As depicted in Supporting Information Fig. S35,

following the addition of **HDB-EtCl**, the fluorescent signals within BEAS-2B cells increased gradually over the first 30 min and remained stable from 40 to 120 min. These observations clearly demonstrate that **HDB-EtCl** exhibits good *in situ* fluorescent imaging performance and offers a wide time window for *in situ* imaging of hCYP1A1in living cells, prompting further investigation into the specificity of **HDB-EtCl** towards CYP1A1.

*3.3. **HDB-EtCl** is specifically activated by CYP1A1*

Next, the sensing properties and specificity of **HDB-EtCl** towards CYP1A1 were carefully studied. As shown in Fig. 2A, Supporting Information Figs. S36 and S37, under physiological conditions, **HDB-EtCl** could be readily metabolized by human CYP1A1 to release a single dealkylated metabolite (**HDBI**), which emitted bright red fluorescent signal around 585 nm. Subsequently, the specificity of **HDB-EtCl** towards CYP1A1 was assessed by performing P450 enzyme reaction phenotyping assays and chemical inhibition assays. As depicted in Fig. 2B, among all tested P450 isoenzymes, only CYP1A1 induced the formation of **HDBI** following 30-minute incubation. Chemical inhibition assays (Fig. 2C) showed that 1-aminobenzotriazole (ABT), a broad-spectrum CYP inhibitor, and resveratrol, an inhibitor of CYP1A1, completely blocked **HDB-EtCl** *O*-dechloroethylation in HLMs, while the inhibitors of other CYPs had negligible inhibition on this reaction. These findings strongly supported that **HDB-EtCl** could be specifically metabolized by CYP1A1 to release a metabolically stable metabolite, **HDBI**. Furthermore, the abundant endogenous substances and cations in biological samples could not influence CYP1A1-catalyzed **HDB-EtCl** *O*-dechloroethylation under physiological conditions (Supporting Information Fig. S38). These observations clearly demonstrate that **HDB-EtCl** is an isoform-specific fluorogenic substrate for CYP1A1, which offers a critical foundation for constructing a practical and reliable cell-based fluorimetric assay for long-term functional imaging of CYP1A1 in living systems, as well as for high-throughput screening of CYP1A1 modulators in living cells.

3.4. In-situ functional imaging of CYP1A1 in living cells and tissue slices

Considering that AhR and CYP1A1 are widely expressed in a variety of cell types and are associated with inflammation in various organs (such as intestine, lung, skin, and liver),

HDB-EtCl is utilized for *in-situ* functional imaging of CYP1A1 in multiple human cell lines, including Caco2, BEAS-2B, H292, and HepG2 cells. Prior to imaging, the cytotoxicity of **HDB-EtCl**, **HDBI**, and resveratrol (a selective CYP1A1 inhibitor) was tested. The results showed that these three compounds exhibited weak cytotoxicity towards all tested mammalian cells (Supporting Information Figs. S39–S42).

As shown in Fig. 3, after 30-minute staining with **HDB-EtCl**, bright fluorescent signals (red channel) were detected within Caco2, BEAS-2B, H292, and HepG2 cells, with high spatial imaging resolution and a high signal-to-noise ratio. Notably, the fluorescent signals (red channel) from these cells could be completely blocked by resveratrol (100 μmol/L). Encouraged by the exceptional imaging performance of **HDB-EtCl** in living cells, the imaging performance of endogenous CYP1A1 in mouse liver/lung slices was further studied using **HDB-EtCl** as a molecular tool.

As depicted in Fig. 4, following staining with **HDB-EtCl** for 30 min under physiological conditions, bright red fluorescent signals were readily captured from the mouse liver/lung slices, while the red fluorogenic signals were merged well with the Hoechst 33342 dye. As expected, the red fluorogenic signals in liver/lung slices could be significantly blocked by resveratrol (100 μmol/L). These observations suggest that **HDB-EtCl** is a practical and reliable functional imaging tool for visualizing mammalian CYP1A1 in living cells and tissue slices, which impel us to construct a practical cell-based biochemical assay for screening and discovering the CYP1A1 modulators at the cellular level.

3.5. Screening the modulators of the AhR-CYP1A1 axis

Considering the critical role of the AhR–CYP1A1 axis in regulating inflammatory and immune diseases, efficacious modulators of this axis are highly desirable for combating these conditions[15,21,49]. CYP1A1 is a key downstream gene product of AhR and an important phenotypic marker of AhR activation. Additionally, it acts as a crucial mediator of various inflammatory diseases[36,37]. Thus, *in situ* visualization of the dynamic changes in CYP1A1 function in living systems offers an alternative way for precisely assessing the outcomes of tested chemicals. To achieve this end, **HDB-EtCl** was used to establish a cell-based fluorimetric assay for high-throughput screening of CYP1A1 inducers (Fig. 5A). To validate

the applicability of **HDB-EtCl** based fluorimetric assay for screening CYP1A1 inducers in living cells, Bap (a known CYP1A1 inducer) was co-cultured with BEAS-2B cells 24 h, a significant enhancement in the red fluorescence signal of **HDBI** was observed inside from BEAS-2B cells (Fig. 5B and C).

Next, we screened the regulatory effects of more than 100 compounds on CYP1A1 from an in-house compound library. The commercially unavailable compounds were fully characterized (Supporting Information Scheme S6 and Figs. S43–S146). As shown in Fig. 5D and Supporting Information Table S4, **LAC-7** showed the strongest CYP1A1 induction effect (a 3.11-fold enhancement in CYP1A1 activity) compared to the positive inducer and other compounds. Furthermore, **LAC-7** upregulated the protein levels of CYP1A1 (2.94-fold) after 24 h induction (Fig. 5E and F). Given the pivotal role of macrophages in inflammatory diseases, the inductive effects of **LAC-7** on CYP1A1 expression in macrophages were investigated using **HDB-EtCl** as a fluorescent substrate. Prior to cell-based assays, the cytotoxicity of **LAC-7** towards BEAS-2B, RAW264.7, and 293T-AhR-luc cells were tested. As shown in Supporting Information Fig. S147, **LAC-7** displayed weak cytotoxicity towards these cells. As demonstrated in Fig. 5G, weak red fluorescent signals were observed in RAW264.7 cells without **LAC-7** treatment. In sharp contrast, strong red fluorescent signals were observed in **LAC-7** treated RAW264.7 cells. Additionally, an AhR luciferase reporter assay also revealed that **LAC-7** could activate AhR transcriptional activity and upregulate AhR expression level in dose-dependent manners (Fig. 6A and B, and Supporting Information Fig. S148). It was also found that **HDB-EtCl** and **HDBI** did not trigger any changes in intracellular AhR expression, and these agents were not the substrate for P-gp (Supporting Information Fig. S149). Meanwhile, it was also found that **LAC-7** showed good metabolic stability in human liver microsomes ($t_{1/2}$ > 120 min), which was much longer than that of the reference drug (testosterone) (Supporting Information Fig. S150). These findings suggest that **HDB-EtCl** can be used as a practical tool for rapid screening and *in-situ* characterization of CYP1A1 inducers in live cells. Moreover, **LAC-7** is identified as an efficacious activator of the AhR-CYP1A1 axis, which can also significantly enhance the expression of both CYP1A1 and AhR in BEAS-2B cells and macrophages.

Prior to the animal tests, the anti-inflammatory effects of **LAC-7** were examined in

LPS-stimulated bone marrow-derived macrophages (BMDMs). As shown in Fig. 6C and D**,** compared to the control group, LPS facilitated macrophage M1 polarization, evidenced by the elevated expression of the M1-specific marker CD86, the diminished expression of the M2-specific marker CD206, and the increased secretion of pro-inflammatory cytokines such as IL-6, TNF-α, IFN-γ, and IL-1β. As expected, **LAC-7** significantly reduced the expression levels of the M1 marker CD86 and upregulated the expression levels of the M2 marker CD206 in LPS-induced BMDMs. Additionally, the levels of IL-6, TNF-α, IFN-γ, and IL-1β were dramatically decreased (Fig. 6C and D).

*3.6. **LAC-7** shows good safety profiles and favorable tissue distribution*

The safety and tissue distribution of **LAC-7** in mice were carefully evaluated prior to *in vivo* studies on its anti-inflammatory effects. Initially, oral administration of **LAC-7** at a high dose (100 mg/kg per day) for 14 consecutive days in healthy mice resulted in no mortality, and the body weight of the mice showed a gradual increase (Fig. 7A and B). Additionally, biochemical assays and hematoxylin and eosin (H&E) staining (Fig. 7C and D) demonstrated that no haematotoxicity, organ injuries, or apparent abnormalities were observed in the **LAC-7**-treated mice, indicating that **LAC-7** possessed a favorable safety profile. Meanwhile, the tissue distribution of **LAC-7** was investigated following a single oral dose (40 mg/kg) in mice. As shown in Supporting Information Fig. S151, **LAC-7** exhibited high exposure in the intestinal tract (including the duodenum, jejunum, ileum, and colon) and was also detectable in the lung and liver tissues. These findings support the further investigation of the anti-inflammatory effects of **LAC-7** in mice.

*3.7. **LAC-7** significantly alleviates DSS-induced ulcerative colitis*

Notably, **LAC-7** was mainly exposed to barrier organs such as the intestinal tract and lung, prompting further investigation into its anti-inflammatory effects in mouse models of ulcerative colitis (UC) and acute lung injury (ALI). To further evaluate the therapeutic potential of **LAC-7** in ulcerative colitis mice, its alleviative effects on DSS-induced ulcerative colitis were investigated. In the model group, DSS-induced mice manifested severe colitis, as indicated by body weight loss, diarrhea, and bleeding (Fig. 8A–D). Compared to

the DSS-treated group, **LAC-7** (20 and 40 mg/kg) treatment significantly reversed DSS-challenged ulcerative colitis, including body weight loss, diarrhea, and bleeding.

DSS significantly shortened the colonic length (a typical indicator of colitis severity) in DSS-treated mice. By contrast, oral administration of **LAC-7** (20 and 40 mg/kg) or salazosulfapyridine (SASP, a positive drug for ulcerative colitis) significantly reversed the shortening of colon length by DSS (Fig. 8C). Pathological conditions in the intestinal tissues were also assessed using hematoxylin-eosin (H&E) staining (Fig. 8E). Compared to the control group, the colonic mucosa of DSS-challenged mice showed severe epithelial disruption, inflammatory cell infiltration, mucous membrane damage, and crypt damage. However, these histopathological abnormities were largely restored in mice treated with **LAC-7** (20 and 40 mg/kg) and SASP. Pro-inflammatory cytokines play a critical role in DSS-induced ulcerative colitis. The expression levels of IL-1β, TNF-α, IL-6, and IFN-γ in intestinal tissues were quantified using commercial ELISA kits. As expected, compared to the control group, the levels of pro-inflammatory cytokines, including IL-1β, TNF-α, IL-6, and IFN-γ, were significantly elevated in the intestine of DSS-induced ulcerative colitis mice (Fig. 8F). In contrast, oral administration of **LAC-7** and SASP effectively mitigated the elevated levels of these cytokines induced by DSS, confirming the excellent anti-inflammatory effects of this agent in ulcerative colitis mice.

The expression levels of tight junction proteins, Occludin and ZO-1, significantly decreased in the intestines of DSS-challenged mice. However, treatment with **LAC-7** and SASP significantly increased the expression of these proteins, thereby restoring the integrity of the intestinal mucosal barrier (Supporting Information Fig. S152). Furthermore, the protein levels of AhR and CYP1A1 in intestinal tissues of DSS-challenged mice were significantly downregulated compared to the control group (Fig. 8G). In contrast, **LAC-7** significantly upregulated the expression levels of both AhR and CYP1A1 in DSS-challenged ulcerative colitis mice, suggesting that **LAC-7** could effectively activate the AhR-CYP1A1 axis. Notably, **LAC-7** (40 mg/kg) demonstrates comparable efficacy to the positive control drug SASP (200 mg/kg) in relieving DSS-induced ulcerative colitis, suggesting that **LAC-7** is a highly efficacious anti-inflammatory agent for treating ulcerative colitis.

*3.8. **LAC-7** significantly attenuates LPS-induced ALI in mice*

Following a single oral administration to mice, **LAC-7** was distributed in lung tissue, in addition to being highly distributed in intestinal tissue. The mitigation effects of **LAC-7** (20 and 40 mg/kg) on LPS-challenged ALI mice were thoroughly investigated. The flowchart detailing the animal experiment protocol is illustrated in Fig. 9A. The ALI model was established in mice *via* intratracheal instillation of LPS, and significant infiltration of inflammatory cells was observed in lung tissue of ALI mice *via* H&E staining (Fig. 9B). In contrast, treatment with both **LAC-7** (20 and 40 mg/kg) and dexamethasone (Dex, a positive control for ALI) significantly ameliorated LPS-induced interstitial edema, infiltration of inflammatory cells, thickening of alveolar walls, and alveolar collapse in mice. Furthermore, both **LAC-7** (20 and 40 mg/kg) and Dex could significantly reduce lung injury scores in ALI mice.

The bronchoalveolar lavage fluid (BALF) experiment was used to evaluate the inflammatory response in lung diseases. Pulmonary alveoli permeability was evaluated based on cell counts in BALF, which were significantly increased in LPS-induced mice. Remarkably, the total cell count in BALF was significantly decreased following treatment with **LAC-7** or Dex compared to LPS-induced ALI mice (Fig. 9C). Subsequently, the levels of TNF-α, IL-6, and IL-1β in BALF were detected (Fig. 9C). Compared to the control group, LPS could significantly increase the levels of TNF-α, IL-6, and IL-1β in BALF. Treatment with **LAC-7** decreased the levels of the cytokine in BALF compared to LPS alone, indicating that **LAC-7** effectively inhibited cytokine secretion in BALF.

Immunofluorescence (IF) analysis was performed to explore the distribution and expression of the tight junction proteins (Occludin and ZO-1) in lung tissues. Mouse lung tissues were stained with an anti-CD31 antibody (green) to visualize endothelial cells. The findings (Fig. 9D) revealed that in the control group, ZO-1 (red) in CD31-positive cells exhibited strong fluorescence intensity and formed a continuous line along the cell boundaries. However, following LPS-induced ALI, the fluorescence intensity of ZO-1 was significantly decreased and displayed a fragmented staining pattern. Remarkably, oral administration of **LAC-7** and Dex significantly increased the immunofluorescence intensity,

with a restoration of continuous cell membrane staining. Similarly, treatment with **LAC-7** or Dex enhanced the immunofluorescence intensity of Occludin, partially restoring cell membrane integrity. Furthermore, **LAC-7** could significantly upregulate the expression of both AhR and CYP1A1 in lung tissues of LPS-induced mice (Supporting Information Fig. S153). These findings clearly demonstrate that **LAC-7** markedly activates the AhR-CYP1A1 axis and attenuates LPS-induced ALI and inflammatory responses in mice, showcasing its impressive anti-inflammatory performance both *in vitro* and *in vivo*.

Inflammatory-related diseases are key contributors to high global mortality and adversely impact quality of life. More than 50% of all deaths are attributed to inflammation-related diseases (such as inflammatory bowel disease (IBD), ischemic heart disease, hypertension, stroke, diabetes mellitus, chronic kidney disease, neurodegenerative disorders, and cancer)[50,51]. Initially, researchers generally believed that AhR was primarily involved in the metabolism of environmental chemicals[26-28]. However, recent evidence suggests that the AhR–CYP1A axis is a therapeutic target for treating autoimmune inflammatory diseases. Activation of this axis in specific cellular environments is emerging as a novel therapeutic modality for various inflammatory diseases, including intestinal inflammation, skin inflammation, acute lung injury, and acute renal injury[30-33].

Previous studies have shown that a variety of compounds (such as I3C) can prevent and treat inflammatory diseases by activating AhR and CYP1A1[52-55]. It is well known that CYP1A1 is the downstream protein of AhR, and CYP1A1 enzymatic activity is critical for restoring epithelial barriers, including the intestine, lung, and skin barriers. Recent studies have also found that the expression of CYP1A1 is crucial for enhancing intestinal and lung barrier functions and for ulcerative colitis and lung protective activity mediated by AhR agonists. This key enzyme promotes M2 macrophage polarization, thereby regulating inflammatory responses[56].

Furthermore, CYP1A1 modulates inflammatory responses by catalyzing the oxidative metabolism of endogenous substances (such as estradiol), herbal constituents, and therapeutic agents[21,22]. For example, CYP1A1 can metabolize estradiol to form 2-hydroxy estradiol, which exerts anti-inflammatory and anti-oxidative stress effects by competitively inhibiting prostaglandin-endoperoxide synthase (PTGS). Notably, some CYP1A1 inhibitors also act as

AhR activators, leading to contradictory findings in target-based biochemical assays and *in vivo* studies. This highlights the need to discover effective modulators of the AhR-CYP1A1 axis by optimized fluorometric cell-based assays combined with the cell-based AhR luciferase reporter assays.

Although various fluorogenic substrates for CYP1A1 have been reported over the past decade, most suffer from poor isoform specificity, limited sensitivity, poor solubility, and inadequate cell membrane permeability. To address these issues, a rational molecule design and cell-based screening strategy are used to develop CYP1A1-specific fluorescent substrates for *in-situ* functional imaging. Fortunately, **HDB-EtCl** was identified as an isoform-specific fluorescent substrate for CYP1A1, demonstrating exceptional real-time fluorescent imaging capabilities in living cells. **HDB-EtCl** showed good cell membrane permeability, while **HDBI,** the metabolites of **HDB-EtCl,** showed favorable optical properties and metabolic stability. As depicted in Fig. S35, **HDB-EtCl** enabled continuous real-time imaging of CYP1A1 in living cells, with stable fluorescence for up to 120 min. Importantly, neither **HDB-EtCl** nor **HDBI** induced CYP1A1 expression by agonizing AhR.

These findings clearly demonstrate that **HDB-EtCl** is an isoform-specific fluorogenic substrate for CYP1A1, offering a critical foundation for constructing a practical and reliable cell-based fluorimetric assay for long-term functional imaging of CYP1A1 in living systems, as well as for high-throughput screening of CYP1A1 modulators in living cells. Typically, detecting CYP1A1 activity in live cells requires cell disruption, leading to results that may not accurately reflect the activity of CYP1A1 in a living system. Therefore, the CYP1A1-specific fluorogenic substrate in this study provides a practical tool for quantifying the activity and function of CYP1A1 in living systems. Moreover, **HDB-EtCl** provides a high-throughput and visual method for detecting CYP1A1 activity that is independent of mass spectrometry and liquid chromatography.

To this end, **HDB-EtCl** was used to construct a cell-based fluorimetric assay for high-throughput screening of CYP1A1 inducers. This method employs a high-content imaging system for quantitative detection through fluorescence imaging, offering superior throughput compared to confocal and high-resolution imaging. By screening of an in-house compound library, the chalcone derivative **LAC-7** was identified as a novel efficacious

activator of the AhR-CYP1A1 axis. Further investigations showed that **LAC-7** could induce the expression levels of both CYP1A1 and AhR in multiple cell lines, while also suppressing macrophage M1 polarization and reducing levels of inflammatory factors in LPS-induced BMDMs. Furthermore, animal toxicity studies demonstrated that **LAC-7** possessed a favorable safety profile, with no significant abnormalities or organ injuries following oral administration at a high dose (100 mg/kg per day) for 14 consecutive days. These findings suggest that **LAC-7** has the potential to be developed as a promising anti-inflammation drug candidate.

To confirm the efficacy of **LAC-7**, we further established its anti-inflammation potential in mice models. Considering that AhR and CYP1A1 are widely expressed in a variety of cells and are associated with inflammation in various barrier organs, including the intestine, lung, and skin. Since **LAC-7** was highly exposed to the intestinal tract, lung, and liver following oral administration, *in vivo* studies were conducted using models of DSS-induced UC and LPS-induced ALI. As anticipated, **LAC-7** (administered at a high dose of 40 mg/kg) demonstrated comparable efficacy to the positive control drug in alleviating DSS-induced UC and LPS-induced ALI mice, suggesting that **LAC-7** is a highly efficacious anti-inflammatory agent. Future research should focus on other modifications to **LAC-7** to optimize its drug-like properties and conduct comprehensive anti-inflammatory pharmacological studies. This will facilitate the design and development of novel anti-inflammatory drug candidates for *in vivo* applications.

4. Conclusions

In summary, a practical *in-situ* functional imaging assay for sensing CYP1A1 activities in living systems was developed and applied for the high-throughput discovery of efficacious modulators of the AhR–CYP1A1 axis. Through rational molecule design and two rounds of screening, **HDB-EtCl** was identified as a highly specific CYP1A1-activatable fluorogenic substrate, exhibiting an optimal combination of isoform-specificity, rapid response, excellent cell-membrane permeability, and superior optical properties. Utilizing **HDB-EtCl**, we constructed a cell-based fluorimetric assay for *in-situ* functional imaging of CYP1A1 and high-throughput screening of CYP1A1 modulators in living cells. The optimized fluorimetric

cell-based assay was integrated with a cell-based AhR luciferase reporter assay to discover efficacious modulators of the AhR–CYP1A1 axis. Following screening of an in-house compound library, **LAC-7** was identified as a novel efficacious activator of the AhR–CYP1A1 axis. Further investigations showed that **LAC-7** could induce the expression levels of both CYP1A1 and AhR in multiple cell lines, while suppressing macrophage M1 polarization and reducing the levels of inflammatory factors in LPS-induced BMDMs. *In vivo* studies showed that **LAC-7** significantly alleviated DSS-induced UC and LPS-induced ALI mice, and markedly reduced the inflammatory responses. Collectively, we report an optimized fluorimetric cell-based assay for *in situ* functional imaging of CYP1A1 activities in living systems, providing a practical tool for high-throughput phenotypic screening and characterization of AhR–CYP1A1 axis modulators. Using this optimized assay, we identified **LAC-7** as a novel efficacious activator of the AhR–CYP1A1 axis with impressively anti-inflammatory properties, positioning it as a promising candidate for developing novel anti-inflammatory agents.

Acknowledgments

This study was supported by National Natural Science Foundation of China (Nos. U23A20516, 81922070, 82273897 and 52303191), National Key Research and Development Program of China (No. 2022YFC3502000), Shanghai Science and Technology Innovation Action Plans (21S21900600, China), the Organizational Key Research and Development Program of Shanghai University of Traditional Chinese Medicine (No. 2023YZZ02, China), Shanghai Municipal Health Commission's TCM research project (No. 2022CX005, China), Innovation Team and Talents Cultivation Program of National Administration of Traditional Chinese Medicine (No. ZYYCXTDD-202004, China), the State Key Laboratory of Fine Chemicals, Dalian University of Technology (No. KF 2202, China) and Shanghai University of Traditional Chinese Medicine (No. 2021LK023, China).

Author contributions

Guangbo Ge and Feng Zhang designed the research. Feng Zhang and Bei Zhao carried out the experiments and performed data analysis. Yufan Fan, Jinhui Shi, Lin Chen, Leizhi Xu, Lanhui Qin, and Mengru Sun participated part of the experiments. Guangbo Ge, Feng Zhang, and Bei Zhao wrote the manuscript. Xin Yang, Zhangping Xiao, Hairong Zeng, Hongping Deng, and Xudong Jin revised the manuscript. All of the authors have read and approved the final manuscript.

Conflicts of interest

The authors have no conflicts of interest to declare.

References

1. Esser C, Rannug A. The aryl hydrocarbon receptor in barrier organ physiology, immunology, and toxicology. *Pharmacol Rev* 2015;**67**:259-79.
2. Stockinger B, Di Meglio P, Gialitakis M, Duarte JH. The aryl hydrocarbon receptor: multitasking in the immune system. *Annu Rev Immunol* 2014;**32**:403-32.
3. Congues F, Wang PC, Lee JS, Lin DP, Shahid A, Xie JM, et al. Targeting aryl hydrocarbon receptor to prevent cancer in barrier organs. *Biochem Pharmacol* 2024;**223**:116156.
4. Dai SY, Qu LZ, Li J, Zhang Y, Jiang LY, Wei HD, et al. Structural insight into the ligand binding mechanism of aryl hydrocarbon receptor. *Nat Commun* 2022;**13**:6234.

5. Rejano-Gordillo CM, Marín-Díaz B, Ordiales-Talavero A, Merino JM, González-Rico FJ, Fernández-Salguero PM. From nucleus to organs: insights of aryl hydrocarbon receptor molecular mechanisms. *Int J Mol Sci* 2022;**23**:14919.
6. Cannon AS, Nagarkatti PS, Nagarkatti M. Targeting AhR as a novel therapeutic modality against inflammatory diseases. *Int J Mol Sci* 2021;**23**:288.
7. Riaz F, Pan F, Wei P. Aryl hydrocarbon receptor: The master regulator of immune responses in allergic diseases. *Front Immunol* 2022;**13**:1057555.
8. Denison MS, Nagy SR. Activation of the aryl hydrocarbon receptor by structurally diverse exogenous and endogenous chemicals. *Annu Rev Pharmacol Toxicol* 2003;**43**:309-34.
9. Piwarski SA, Salisbury TB. The effects of environmental aryl hydrocarbon receptor ligands on signalling and cell metabolism in cancer. *Biochem Pharmacol* 2023;**216**:115771.
10. Jeuken A, Keser BJG, Khan E, Brouwer A, Koeman J, Denison MS. Activation of the Ah receptor by extracts of dietary herbal supplements, vegetables, and fruits. *J Agric Food Chem* 2003;**51**:5478-87.
11. Hanieh H, Ismail MB, Alfwuaires MA, Ibrahim HIM, Farhan M. Aryl Hydrocarbon receptor as an anticancer target: an overview of ten years Odyssey. *Molecules* 2023;**28**:3978.
12. Evans BR, Karchner SI, Allan LL, Pollenz RS, Tanguay RL, Jenny MJ, et al. Repression of aryl hydrocarbon receptor (AHR) signalling by AHR repressor: role of DNA binding and competition for AHR nuclear translocator. *Mol Pharmacol* 2008;**73**:387-98.
13. Seok SH, Lee W, Jiang L, Molugu K, Zheng AP, Li YT, et al. Structural hierarchy controlling dimerization and target DNA recognition in the AHR transcriptional complex. *Proc Natl Acad Sci U S A* 2017;**114**:5431-6.
14. Uno S, Nebert DW, Makishima M. Cytochrome P450 1A1 (CYP1A1) protects against nonalcoholic fatty liver disease caused by Western diet containing benzo[a]pyrene in mice. *Food Chem Toxicol* 2018;**113**:73-82.
15. Tian WZ, Yue Q, Fei W, Yao PZ, Han RQ, Tang JG. PE (0:0/14:0), an endogenous metabolite of the gut microbiota, exerts protective effects against sepsis-induced intestinal injury by modulating the AHR/CYP1A1 pathway. *Clin Sci (Lond)* 2023:**137**:1753-69.
16. Kwon YJ, Shin S, Chun YJ. Biological roles of cytochrome P450 1A1, 1A2, and 1B1 enzymes. *Arch Pharm Res* 2021;**44**:63-83.
17. Schiering C, Wincent E, Metidji A, Iseppon A, Li Y, Potocnik AJ, et al. Feedback control of AHR signalling regulates intestinal immunity. *Nature* 2017;**542**:242-5.
18. Wincent E, Kubota A, Timme-Laragy A, Jönsson ME, Hahn ME, Stegeman JJ. Biological effects of 6-formylindolo[3,2-*b*]carbazole (FICZ) *in vivo* are enhanced by loss of CYP1A function in an Ahr2-dependent manner. *Biochem Pharmacol* 2016;**110-111**:117-29.
19. Wincent E, Bengtsson J, Bardbori AM, Alsberg T, Luecke S, Rannug U, et al. Inhibition of cytochrome P4501-dependent clearance of the endogenous agonist FICZ as a mechanism for activation of the aryl hydrocarbon receptor. *Proc Natl Acad Sci U S A* 2012;**109**:4479-84.
20. Song MM, Sheng XJ, Zhang JR, Li XR, Dai QY, Chen Y, et al. Homeostatic regulation of the aryl hydrocarbon receptor-cytochrome P450 1a axis by Scutellaria baicalensis-Coptis chinensis herb pair and its main constituents. *J Ethnopharmacol* 2022;**297**:115545.
21. Kamel M, Shouman S, El-Merzebany M, Kilic G, Veenstra T, Saeed M, et al. Effect of tumour necrosis factor-alpha on estrogen metabolic pathways in breast cancer cells. *J Cancer* 2012;**3**:310-21.
22. Higuchi A, Oonishi E, Kawakita T, Tsubota K. Evaluation of treatment for dry eye with 2-hydroxyestradiol using a dry eye rat model. *Mol Vis* 2016;**22**:446-53.

23. Mimura J, Ema M, Sogawa K, Fujii-Kuriyama Y. Identification of a novel mechanism of regulation of Ah (dioxin) receptor function. *Genes Dev* 1999;**13**:20-5.
24. Coelho NR, Pimpão AB, Correia MJ, Rodrigues TC, Monteiro EC, Morello J, et al. Pharmacological blockage of the AHR-CYP1A1 axis: a call for *in vivo* evidence. *J Mol Med (Berl)* 2022;**100**:215-243.
25. Shinde R, McGaha TL. The Aryl Hydrocarbon receptor: connecting immunity to the microenvironment. *Trends Immunol* 2018;**39**:1005-20.
26. Rayan M, Sayed TS, Hussein OJ, Therachiyil L, Maayah ZH, Maccalli C, et al. Unlocking the secrets: exploring the influence of the aryl hydrocarbon receptor and microbiome on cancer development. *Cell Mol Biol Lett* 2024;**29**:33.
27. Sweeney C, Lazennec G, Vogel CFA. Environmental exposure and the role of AhR in the tumor microenvironment of breast cancer. *Front Pharmacol* 2022;**13**:1095289.
28. Zhao H, Chen L, Yang T, Feng YL, Vaziri ND, Liu BL, et al. Aryl hydrocarbon receptor activation mediates kidney disease and renal cell carcinoma. *J Transl Med* 2019;**17**:302.
29. Priya DKD, Gayathri R, Sakthisekaran D. Role of sulforaphane in the anti-initiating mechanism of lung carcinogenesis *in vivo* by modulating the metabolic activation and detoxification of benzo(a)pyrene. *Biomed Pharmacother* 2011;**65**:9-16.
30. Pernomian L, Duarte-Silva M, Cardoso CRD. The aryl hydrocarbon receptor (AHR) as a potential target for the control of intestinal inflammation: insights from an immune and bacteria sensor receptor. *Clin Rev Allergy Immunol* 2020;**59**:382-90.
31. Li YY, Wang XJ, Su YL, Wang Q, Huang SW, Pan ZF, et al. Baicalein ameliorates ulcerative colitis by improving intestinal epithelial barrier *via* AhR/IL-22 pathway in ILC3s. *Acta Pharmacol Sin* 2022;**43**:1495-507.
32. Ghosh S, Moorthy B, Haribabu B, Jala VR. Cytochrome P450 1A1 is essential for the microbial metabolite, Urolithin A-mediated protection against colitis. *Front Immunol* 2022;**13**:1004603.
33. Xue X, Xiao Y, Zhu HL, Wang H, Liu YZ, Xie TP, et al. Induction of P450 1A by 3-methylcholanthrene protects mice from aristolochic acid-I-induced acute renal injury. *Nephrol Dial Transplant* 2008;**23**:3074-81.
34. Meynier M, Baudu E, Rolhion N, Defaye M, Straube M, Daugey V, et al. AhR/IL-22 pathway as new target for the treatment of post-infectious irritable bowel syndrome symptoms. *Gut Microbes* 2022;**14**:2022997.
35. Modoux M, Rolhion N, Lefevre JH, Oeuvray C, Nádvorník P, Illes P, et al. Butyrate acts through HDAC inhibition to enhance aryl hydrocarbon receptor activation by gut microbiota-derived ligands. *Gut Microbes* 2022;**14**:2105637.
36. Mescher M, Haarmann-Stemmann T. Modulation of CYP1A1 metabolism: from adverse health effects to chemoprevention and therapeutic options. *Pharmacol Ther* 2018;**187**:71-87.
37. Mattingly CJ, McLachlan JA, Jr Toscano WA. Green fluorescent protein (GFP) as a marker of aryl hydrocarbon receptor (AhR) function in developing zebrafish (Danio rerio). *Environ Health Perspect* 2001;**109**:845-9.
38. Dai ZR, Feng L, Jin Q, Cheng H, Li Y, Ning J, et al. A practical strategy to design and develop an isoform-specific fluorescent probe for a target enzyme: CYP1A1 as a case study. *Chem Sci* 2017;**8**:2795-803.
39. Ji HF, Zhang XX, Dai YP, Xue TZ, Misal S, Qi ZJ. A highly selective ratiometric fluorescent probe based on naphthalimide for detection and imaging of CYP1A1 in living cells and zebrafish. *Analyst* 2019;**144**:7390-97.

40. Jin Q, Ma HY, Feng L, Wang P, He RJ, Ning J, et al. Sensing cytochrome P450 1A1 activity by a resorufin-based isoform-specific fluorescent probe, *Chin Chem Lett* 2020;**31**:2945-9.
41. Rahikainen T, Häkkinen MR, Finel M, Pasanen M, Juvonen RO. A high throughput assay for the glucuronidation of 7-hydroxy-4-trifluoromethylcoumarin by recombinant human UDP-glucuronosyltransferases and liver microsomes. *Xenobiotica* 2013;**43**:853-61.
42. Lv X, Ge GB, Feng L, Troberg J, Hu LH, Hou J, et al. An optimized ratiometric fluorescent probe for sensing human UDP-glucuronosyltransferase 1A1 and its biological applications. *Biosens Bioelectron* 2015;**72**:261-7.
43. Liu Y, Luo XM, Yang CX, Yang TY, Zhou JJ, Shi SJ. Impact of quercetin-induced changes in drug-metabolizing enzyme and transporter expression on the pharmacokinetics of cyclosporine in rats. *Mol Med Rep* 2016;**14**:3073-85.
44. Yu TJ, Zhou ZH, Liu SJ, Li CJ, Zhang ZW, Zhang Y, et al. The role of phosphatidylcholine 34:1 in the occurrence, development and treatment of ulcerative colitis. *Acta Pharm Sin B* 2023;**13**:1231-45.
45. Meng Q, Guo JS, Lv K, Liu Y, Zhang J, Li MY, et al. 5S-Heudelotinone alleviates experimental colitis by shaping the immune system and enhancing the intestinal barrier in a gut microbiota-dependent manner. *Acta Pharm Sin B* 2024;**14**:2153-76.
46. Poroyko V, Meng FY, Meliton A, Afonyushkin T, Ulanov A, Semenyuk E, et al. Alterations of lung microbiota in a mouse model of LPS-induced lung injury. *Am J Physiol Lung Cell Mol Physiol* 2015;**309**:L76-83.
47. Zhou Y, Li PF, Goodwin A, Cook J, Halushka P, Chang E, et al. Exosomes from endothelial progenitor cells improve outcomes of the lipopolysaccharide-induced acute lung injury. *Crit Care* 2019;**23**:44.
48. Ning J, Tian ZH, Wang B, Ge GB, An Y, Hou J, et al. A highly sensitive and selective two-photon fluorescent probe for real-time sensing of cytochrome P450 1A1 in living systems, *Mater Chem Front* 2018;**2**:2013–20.
49. Hao T, Zhang R, Zhao T, Wu J, Leung WK, Yang J, et al. Porphyromonas gingivalis infection promotes inflammation *via* inhibition of the AhR signaling pathway in periodontitis. *Cell Prolif* 2023;**56**:e13364.
50. Li T, Liu ZY, Hu JL, Chen L, Chen TT, Tang QQ, et al. A universal chemotactic targeted delivery strategy for inflammatory diseases. *Adv Mater* 2022;**34**:e2206654.
51. Shields GS, Spahr CM, Slavich GM. Psychosocial interventions and immune system function: a systematic review and meta-analysis of randomized clinical trials. *JAMA Psychiatry* 2020;**77**:1031-43.
52. Hu XC, Xiao WF, Lei YX, Green A, Lee X, Maradana MR, et al. Aryl hydrocarbon receptor utilises cellular zinc signals to maintain the gut epithelial barrier. *Nat Commun* 2023;**14**:5431.
53. Major J, Crotta S, Finsterbusch K, Chakravarty P, Shah K, Frederico B, et al. Endothelial AHR activity prevents lung barrier disruption in viral infection. *Nature* 2023;**621**:813-20.
54. Wiggins BG, Wang YF, Burke A, Grunberg N, Walker JMV, Dore M, et al. Endothelial sensing of AHR ligands regulates intestinal homeostasis. *Nature* 2023;**621**:821-9.
55. Liu Y, Bai X, Wu HY, Duan ZG, Zhu CH, Fu RZ, et al. Ginsenoside CK alleviates DSS-induced IBD in mice by regulating tryptophan metabolism and activating aryl hydrocarbon receptor *via* gut microbiota modulation. *J Agric Food Chem* 2024;**72**:9867-79.
56. Zhou XY, Tian LX, Huang Q, Liang H. Research progress on the relationship between cytochrome P4501A1 (CYP1A1) and immune diseases. *Infect Inflamm Rep* 2017;**18**:120-4.

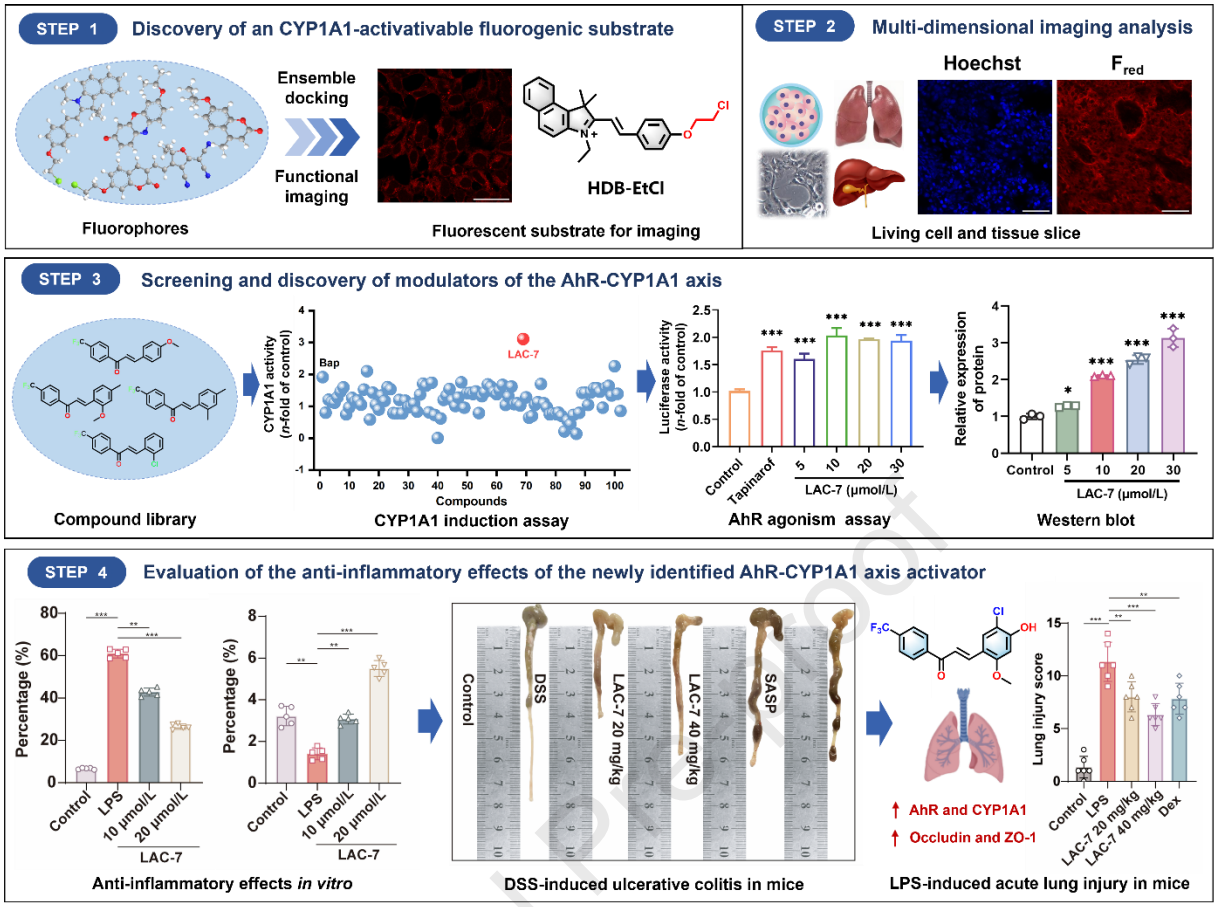

Scheme 1 Schematic illustration of the construction of an optimized fluorometric cell-based assay for discovering potent activators of the AhR–CYP1A1 axis as efficacious anti-inflammatory agents.

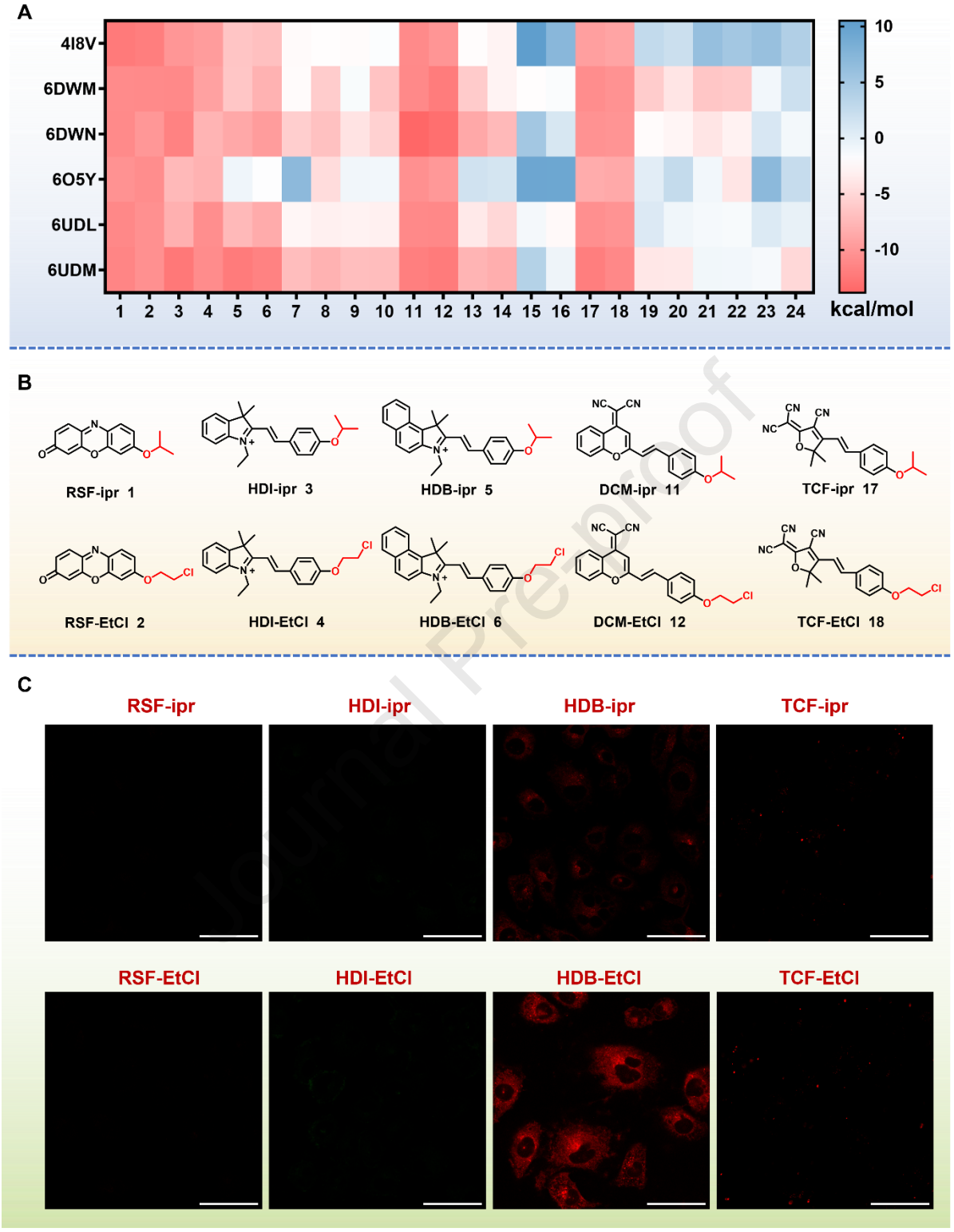

Figure 1 (A) Predicting the binding-affinity (the first conformation) of 24 fluorophores towards hCYP1A1 by ensemble docking. (B) Chemical structures of 10 fluorescent substrate candidates for CYP1A1. (C) Functional imaging for CYP1A1 in BEAS-2B cells by using 10 fluorescent substrate candidates. Scale bar: 50 μm. Data are presented as mean ± SD (n = 3).

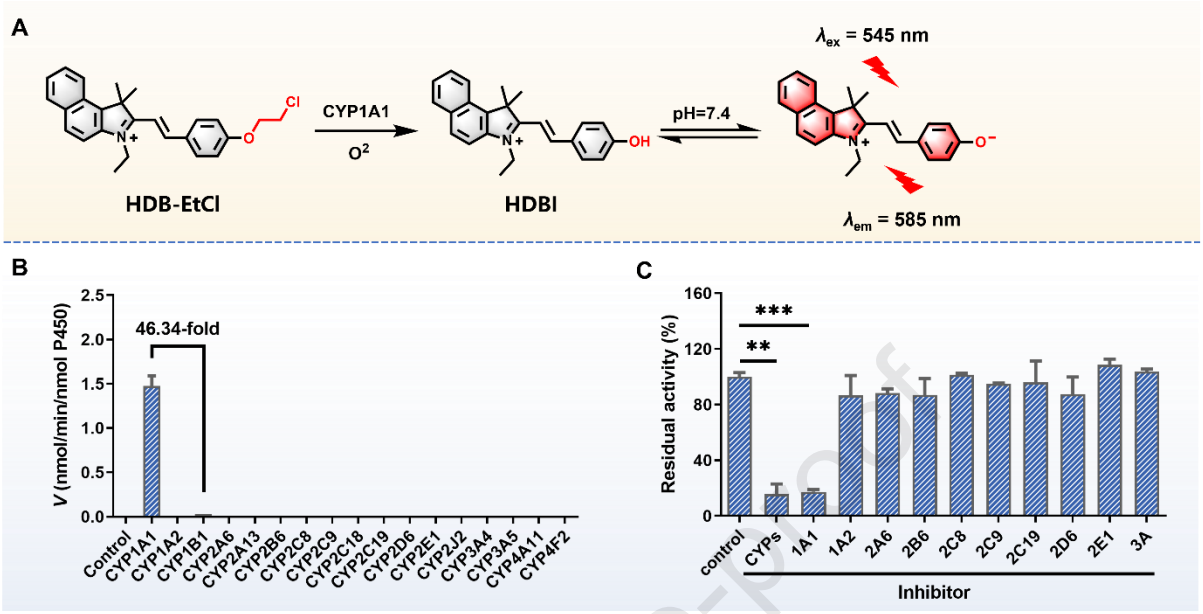

Figure 2 (A) Sensing mechanism of **HDB-EtCl** towards hCYP1A1. (B) **HDB-EtCl** was incubated with each tested human CYP enzyme for 30 min under physiological conditions (37 °C, pH 7.4). (C) The inhibitory effects of CYP inhibitors on **HDB-EtCl** *O*-dechloroethylation in human liver preparations. Data are presented as mean ± SD (n = 3). $^{**}P < 0.01$, and $^{***}P < 0.001$.

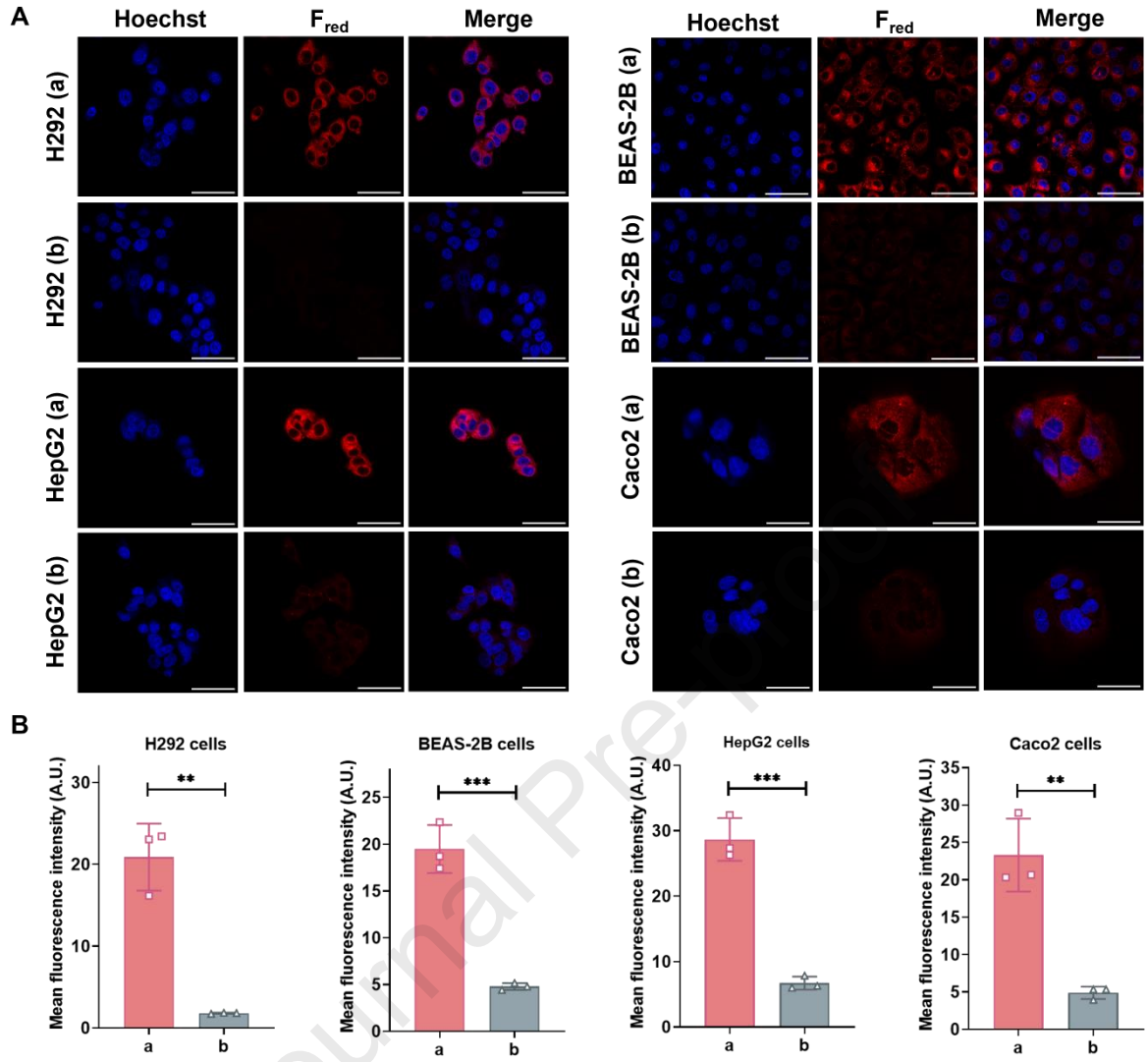

Figure 3 (A) Functional imaging of hCYP1A1 in living cells using confocal laser scanning microscopy. (B) The mean fluorescence intensity of A. (a) The cells were incubated with **HDB-EtCl** (5 μmol/L, red channel) for 30 min, Hoechst 33342 (blue channel) for 15 min. (b) The cells were treated by resveratrol (a hCYP1A1 inhibitor, 100 μmol/L) for 1 h, following staining by **HDB-EtCl**. Data are presented as mean ± SD (n = 3). Scale bar: 50 μm. $^{**}P < 0.01$, and $^{***}P < 0.001$.

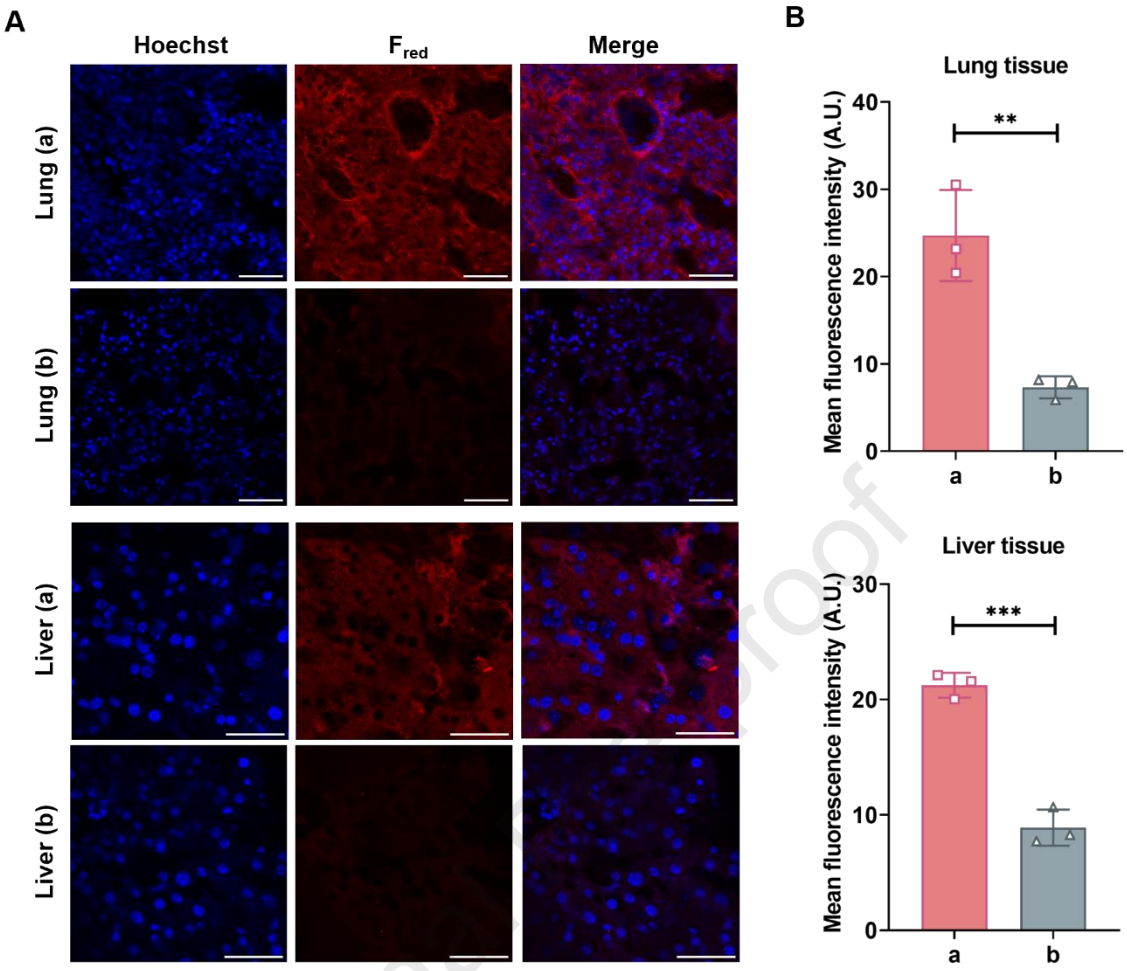

Figure 4 (A) Functional imaging of CYP1A1 in mouse liver and lung slices using confocal laser scanning microscopy. (B) The mean fluorescence intensity of A. (a) The slices were incubated with **HDB-EtCl** (5 μmol/L, red channel) for 30 min, Hoechst 33342 (blue channel) for 15 min. (b) The slices were treated with resveratrol (100 μmol/L) for 1 h, following staining by **HDB-EtCl**. Data are presented as mean ± SD (n = 3). Scale bar: 50 μm. $^{**}P < 0.01$, and $^{***}P < 0.001$.

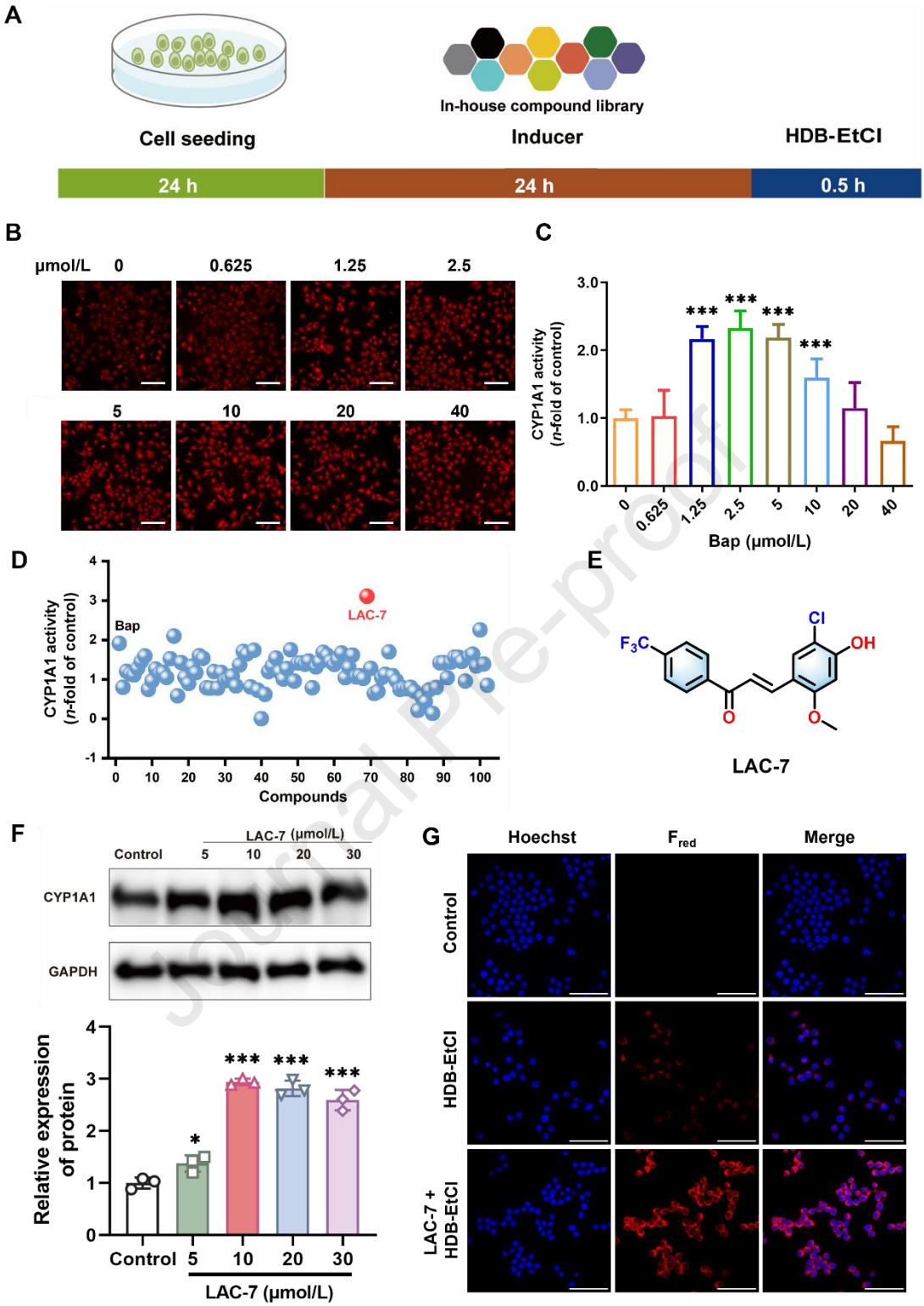

Figure 5 (A) Schematic diagram for screening CYP1A1 inducers. (B, C) Evaluation of the inductive effect of Bap (a reported CYP1A1 inducer) on CYP1A1 in BEAS-2B cells. Scale bar: 150 μm. (D) The hCYP1A1-induction potentials of an in-house compound library using **HDB-EtCl** as the fluorogenic substrate. (E) The structure of **LAC-7**. (F) Quantification of the CYP1A1 levels in BEAS-2B cells with or without **LAC-7**. (G) Functional imaging of

CYP1A1 with or without **LAC-7** induced CYP1A1 in RAW264.7 cells. Scale bar: 50 μm. Data are presented as mean ± SD (n = 3). *P < 0.05, and ***P < 0.001.

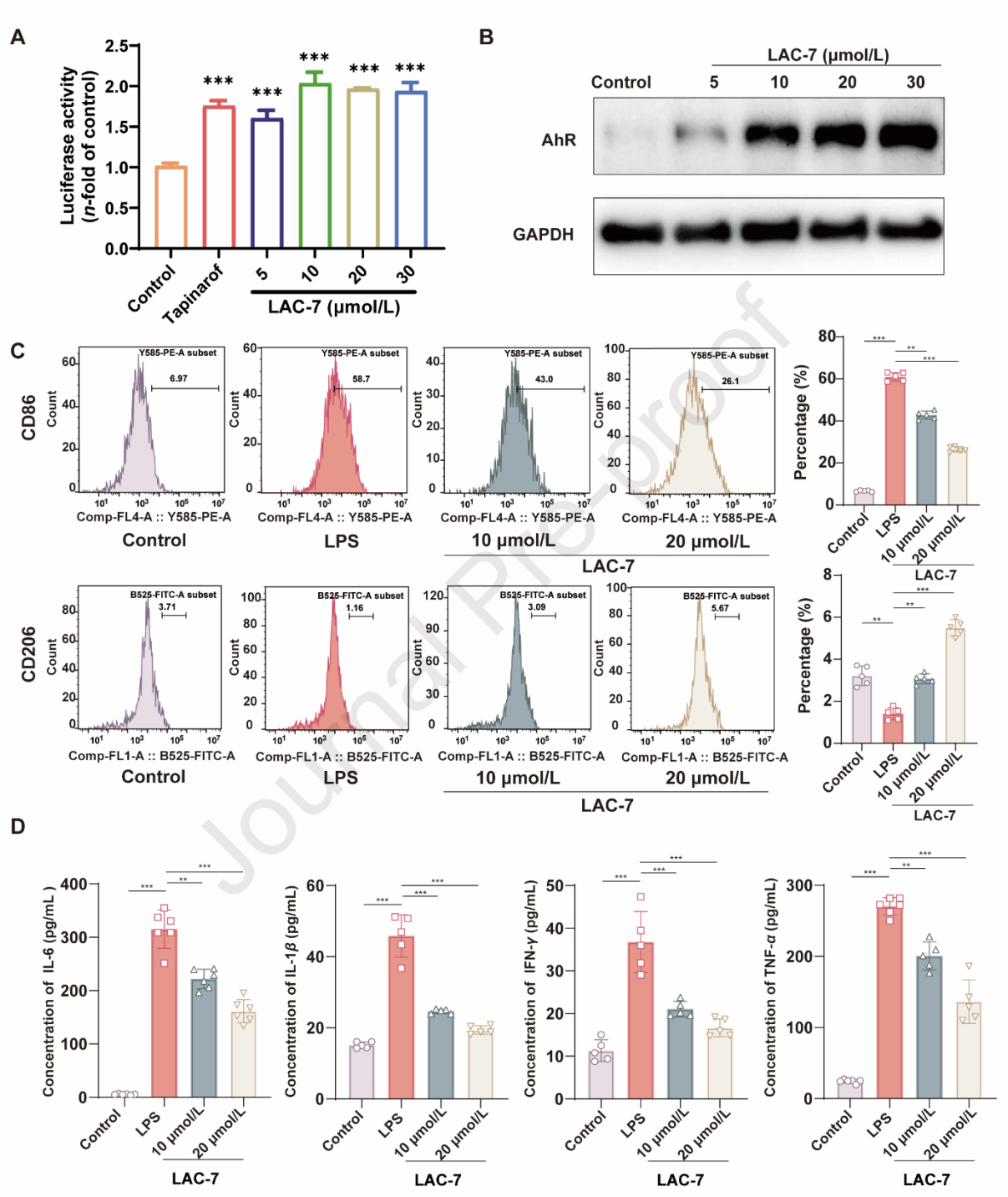

Figure 6 (A) The agonistic effects of **LAC-7** on AhR. (B) WB plot of **LAC-7** induced AhR in BEAS-2B cells. (C) Flow cytometry analysis and quantitative analysis of M1 marker CD86 and M2 marker CD206 in Bone Marrow-Derived Macrophages (BMDMs) following **LAC-7** treatment. (D) **LAC-7** significantly reduced the levels of IL-6, IL-1β, IFN-γ, TNF-α

in LPS-induced BMDMs. Data are presented as mean ± SD (n = 3 or 5). **P < 0.01, and ***P < 0.001.

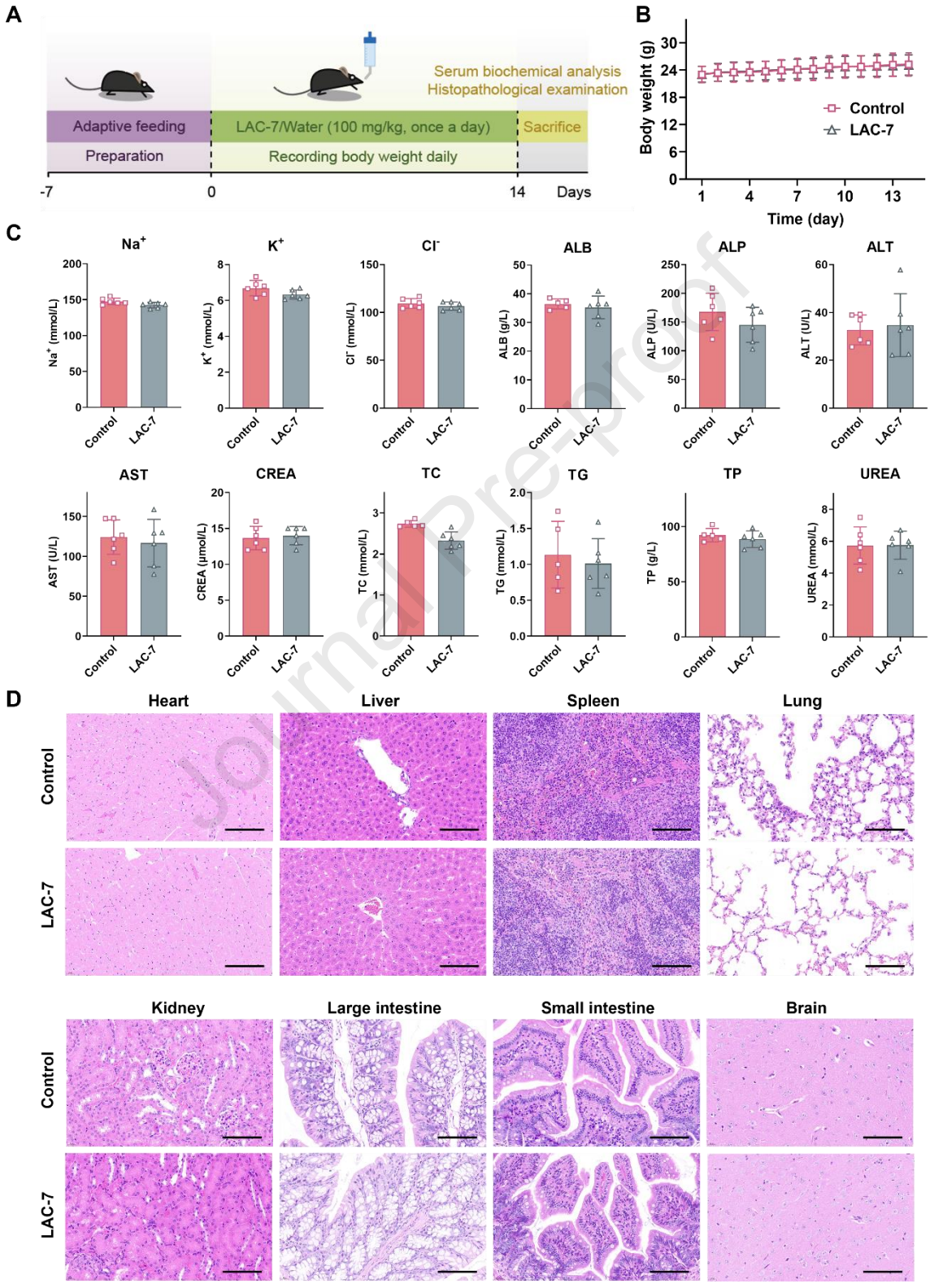

Figure 7 **LAC-7** shows good safety profiles in mice. (A) Animal experimental road map.

(B) Body weight changes in mice. (C) The serum biochemical analysis in control and **LAC-7** groups. (D) Typical hematoxylin and eosin (H&E) staining from control and **LAC-7** groups. Scale bar: 100 μm. Data are presented as mean ± SD (*n* = 5 or 6).

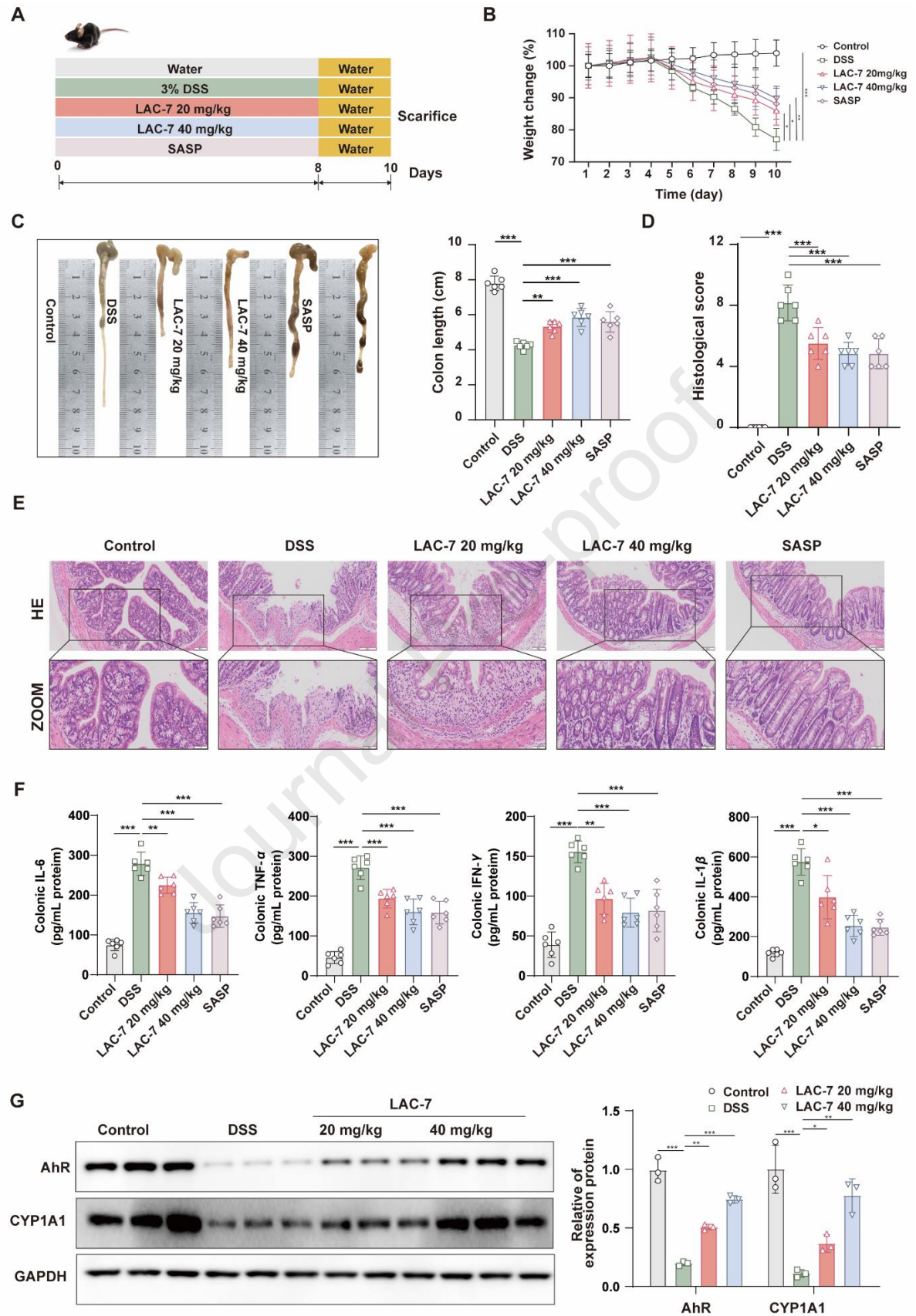

Figure 8 Treatment outcomes of **LAC-7** on DSS-induced ulcerative colitis in mice. (A) Timeline for the establishment of the ulcerative colitis model and **LAC-7** treatment. (B) The

weight change of each group mice following **LAC-7** treatment. (C) The colon length of each group mice following **LAC-7** treatment. (D) The histological score of mice in each group. (E) HE-stained colon tissue sections. Scale bar: 100, 50 μm. (F) Level of proinflammatory cytokines (IL-6, TNF-α, IFN-γ, IL-1β). (G) Effect of **LAC-7** on CYP1A1 and AhR protein expression in colon tissues. Data are presented as mean ± SD (n = 3 or 6). *P < 0.05, **P < 0.01, and ***P < 0.001.

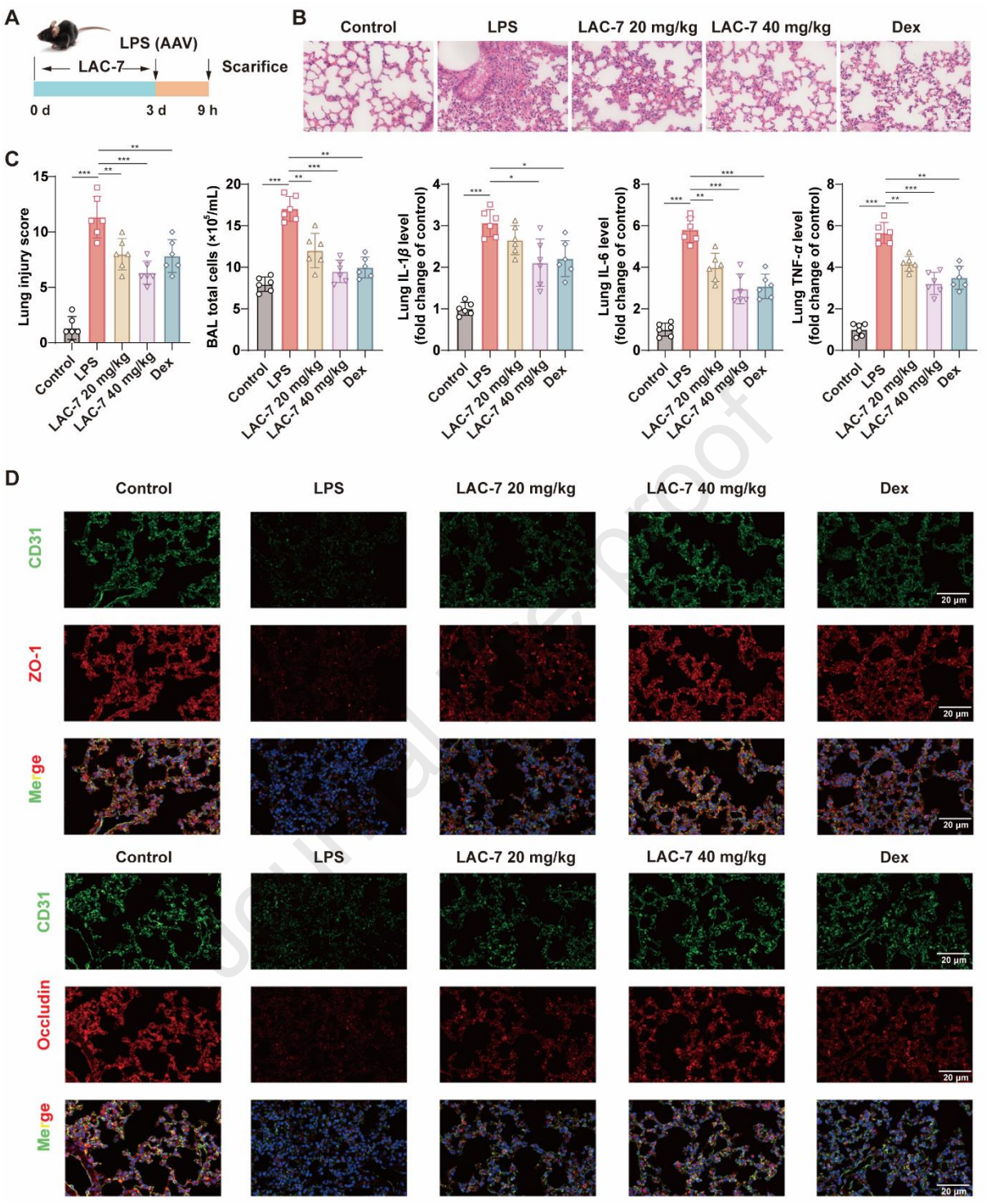

Figure 9 Therapeutic effects of **LAC-7** on LPS-induced acute lung injury (ALI) in mice. (A) Timeline for the establishment of the ALI model and **LAC-7** treatment. (B) HE-stained lung sections. Scale bar: 50 μm. (C) Effects of **LAC-7** on BALF total cells and proinflammatory cytokines levels (IL-1β, IL-6, TNF-α). (D) Immunofluorescence plots of CD31 and two tight junction proteins (ZO-1 and Occludin) in LPS-induced ALI mice and **LAC-7** treated group. Scale bar: 20 μm. Data are presented as mean ± SD (n = 6). *P < 0.05,

**$P < 0.01$, and ***$P < 0.001$.